Pore Characteristics and Computed Permeability of Pastes Subject to Freeze-thaw Cycles at Very Early Ages by X-ray CT

Y. Wei, Z. Wu and X. Gao
Department of Civil Engineering, Tsinghua University, Beijing, China

ABSTRACT

Freeze-thaw cycling can damage microstructure of concrete and reduce the service life of concrete structures. This is especially detrimental for concrete subject to freeze-thaw cycles at very early-ages, such as within the first few days after constructions. Typical low and high water-to-cement (w/c) ratio pastes are investigated experimentally and numerically in this study. The pastes are subject to freeze-thaw cycles at the age of 1, and 7 days and then sealed-cured to the age of 45 days. The pore size distribution is measured and quantified by X-ray computer tomography (CT) with high resolution. The permeability of the corresponding pastes is predicted numerically based on the reconstructed microstructure results obtained from the CT measurements. The pore size distribution and the permeability variations of different pastes are investigated, and the key affecting factors are recognized. The Katz-Thompson and Navier-Stokes methods for computing permeability of paste are compared. The detectable pore size range by MIP, BSE, and X-ray CT in hardened paste is identified. The results of this study will offer suggestions for material design and curing strategies for concrete structures which are prone to experiencing freeze-thaw cycles at very early-ages.

Keywords: Early-age concrete; Freeze-thaw cycling, pore; computed permeability; X-ray Computer Tomography.

1.0 INTRODUCTION

Freeze-thaw cycling can damage the microstructure of concrete and reduce the service life of concrete structures. This is especially detrimental for concrete subject to freeze-thaw cycles at very early-ages, such as within the first few days after constructions. This severe condition is typically seen in high altitude and low-temperature area where it can have warm summer-like weather at noon and cool winter-like weather in the morning and evening. The freshly-cast concrete structures in that area are often subject to freeze-thaw cycles even during the first few days. It is of significance to investigate the microstructure and the permeability of such concretes to understand the deterioration mechanism and its consequence on concrete durability performance.

With the advance of technology and the awareness of the effect from the microstructure level, many techniques have been reexamined and combined to explore the mechanism of deterioration of concrete. Limited researches have been conducted to explore the pore evolution in cementitious materials subject to freeze-thaw cycles. Igarashi *et al.* (2005) found that the total porosity estimated from the BSE image analysis was almost the same as the total porosity measured by the MIP method.

As technology in image acquisition, processing, analysis and computational methods continually improve, we could take advantage of the 3D information provided by X-ray micro tomography, not only to visualize, but also to quantify more accurately the air void, cracks, and other properties, such as permeability and to assess the durability performance of cement-based materials against freeze-thaw action.

This study intends to investigate the pore characteristics of concrete structures constructed in Tibetan Plateau where temperature changes significantly during a day. The concrete can experience freeze-thaw cycles shortly after construction. Considering that the Tibetan Plateau is dry, and most of the structures, such as bridges and roads, are not directly exposed to water, an air freeze-thaw testing condition was adopted in this study. Typical low and high *w/c* ratio pastes are investigated experimentally and numerically to evaluate the pore size distribution and the permeability variations of different pastes.

2.0 COMPUTATIONAL METHODS

Permeability is mainly affected by the microstructure of the cementitious materials. Some models have been developed to predict the permeability of porous media by correlating to their microstructural parameters. The Kata-Thompson equation and the Navier-Stokes numerical method are two models which are normally used to predict the permeability of porous medium.

2.1 Katz-Thompson Equation

Katz and Thompson derived an equation relating the permeability of porous media to the microstructural parameters by using percolating concepts in terms of conductivity (1987). Kata-Thompson relationship is one of the models to predict the permeability of sedimentary rock from the mercury intrusion porosimetry (MIP) data. In this relationship, the intrinsic permeability of fluid (k in m^2) is expressed as:

$$k = \frac{1}{226}\frac{\sigma}{\sigma_0}L_c^2 \tag{1}$$

where, σ is the electrical conductivity of the saturated porous materials (S/m), σ_0 is the conductivity of the solution in the pores (S/m), and L_c is the characteristic length scale of the pore space, which corresponds to the pore diameter at the inflection point on a cumulative volume versus pressure diagram measured from MIP test (Cui and Cahyadi 2001), and it is thought that the pore diameter above which a connected path can form spanning the sample.

The smaller the critical pore size, the finer the pore structure. It was experimentally proven by measuring the electrical resistance of the sample, that the inflection point of the rapidly rising portion of the cumulative intrusion curve marks the threshold for the formation of a continuous pathway and consequently electrical continuity through the sample. Therefore, permeability is determined by the connectivity of pore (denoted by σ/σ_0 and often called the conductivity formation factor) and the pertinent length scale (L_c).

Kata and Thompson (1987) proposed an expression for the conductivity formation factor which can be calculated from MIP data as:

$$\frac{\sigma}{\sigma_0} = \frac{L_{\max}^e}{L_c}\phi S\left(L_{\max}^e\right) \tag{2}$$

where, $L_{\max}$ is the electrical conductivity characteristic dimension that produces maximum conductance, ϕ is total porosity, S is fractional volume of connected pore space involving pore diameter of $L_{\max}$ and larger.

2.2 Navier-Stokes Method

Navier-Stokes model was normally used to numerically predict the intrinsic permeability of porous media from the reconstructed 3D microstructures (Sun *et al.* 2014, Das *et al.* 2015, Promentilla *et al.* 2016). The binary image data were used for the permeability solver code. The pore and the solid phases were assigned with black and white colour, respectively. Then the 2D binary images were stacked to obtain the 3D microstructure. The permeability of the reconstructed 3D microstructure containing pores and solids was calculated using the NIST Stokes permeability solver (Bentz and Martys 2007). The idea is to solve the Navier-Stokes equation for the average velocity which is then used for permeability calculation based on Darcy's law. A pressure gradient is applied to a direction with 1 unit per voxel. The fluid velocity vector field due to the applied pressure within each pore voxel is calculated by a finite difference solution for this incompressible steady-state fluid flow. The intrinsic permeability in the direct of flow can be calculated by using Darcy's law when the finite difference solution converges.

3.0 EXPERIMENTAL METHODS

3.1 Materials and Samples

Cement pastes with water-to-cement (*w/c*) ratio of 0.3 and 0.5 were investigated, which represent high and low strength paste, denoted as 3P and 5P, respectively. The cement used was ordinary Portland cement. After mixing, the fresh paste was cast into plastic tubes with diameter of 5 mm for Micro-CT scanning. Another samples were made by casting fresh paste into tubes with dimension of 10 mm for BSE and MIP test. Rotation was done by hand from time to time after casting to avoid excessive bleeding during the setting period, particularly for paste with high *w/c* ratio of 0.5. After initial set, the plastic tubes filled with the hardening paste were placed in a curing room with constant temperature of 20°C and relative humidity of 50% until the age for testing.

3.2 Freeze-Thaw Test

An air freeze-thaw testing condition was adopted in this study. The temperature was set to vary uniformly between – 20 to 20 °C for one cycle, and each cycle is finished within 6 hrs. The freeze-thaw cycles were initiated on pastes at the age of 1, and 7 days, simulating the early-age frozen condition. The freeze-thaw period was last for 12 days for each test, and thus total 48 freeze-thaw cycles were applied to each sample. A control sample which was not subject to freeze-thaw cycles and cured in a sealed condition in the tube placed in the curing room was also tested for comparison. All the paste samples were tested at the age of 45 days for pore size characterization by the techniques of MIP, BSE, and X-ray CT scan.

The sample was denoted as 3P-1d-FT, 3P-7d-FT, representing that freeze-thaw cycling started at the age of 1 and 7 days for *w/c* ratio=0.3 pastes, 3P-control represents the sample under the sealed-cured condition. For *w/c* ratio=0.5 paste, "3P" was replaced by "5P".

3.3 X-ray CT Scanning

Utilizing X-ray CT scanning to obtain the microstructure information is considered more convenient and realistic, because the delicate grinding and polishing processes which were

normally applied to obtain the flat surface before the microstructural observation are not required for X-ray CT scanning, and thus the original microstructure of sample can be preserved without disturbance. However, the reconstruction of the microstructure from the scanned 2D images requires computational skills which might not be mastered by everyone, and the microstructure information revealed normally depends on the spatial resolution of the X-ray CT machine. Currently, the lower limit of the spatial resolution of X-ray CT can be achieved at the magnitude of micrometer level, which is greater than the lower limit of resolution of BSE image. Therefore, only the pore with size at the micrometer can be identified and quantified by X-ray CT scanning.

A Skyscan 1172 X-ray Micro-CT was used to scan the paste sample for pore size distribution, in which a 3D digital image was reconstructed from a series of 2D images within which each pixel has an X-ray absorption value that correlates to the material density, and the microstructure can be pictured based on the arrangement of the voxels. The sample size is Φ5 mm × 10 mm. A power setting of 100 kV and 50 µA was used for a full cone-beam scan with 1284 projection views. The resolution is 2.97µm. Each scan was made every 2.97µm along the height of the sample. The image acquisition time for each sample that includes both scanning and reconstruction was about two hours. A further image processing and analysis was done by using the programs of Mimics and Matlab.

Fig. 1a shows the reconstructed 3D representation of paste. The different phases appear different grey levels, similar to that in BSE image. Large value of the grey level represents higher absorption of the phase with greater density (Bentz *et al.* 2002). From the reconstructed 3D image data set, the cubic volume of interest (VOI) of 300^3 voxels was extracted from the middle of the cylindrical sample, because there is increase in the grey level where close to the boundary of the sample due to ray attenuation, scatter and noise (Hu *et al.* 2015). Total 30 images were scanned within this cubic volume of interest, they were stacked and reconstructed to form a 3D representative of the microstructure. Considering the characteristic length of individual phase in hardened cement paste is about $10^{-6} \sim 10^{-5}$ m (Oliver *et al.* 2003), the reconstructed cubic volume with size of 900 × 900 × 900 µm can represent the homogeneous property of the sample tested. Fig. 1b shows the 3D microstructure of pores. The pore phase was segmented based on the grey value, and the porosity is calculated by dividing the number of pore voxels with the total number of voxels in the volume of interest.

3.4 MIP and BSE

The pore size distribution of pastes subject to freeze-thaw at the age of 1 and 7 days and the paste under sealed curing was also measured by Mercury Intrusion Porosimetry (MIP) and by using FEI QUANTA 200 scanning electron microscopy for backscattered electron image (BSE).
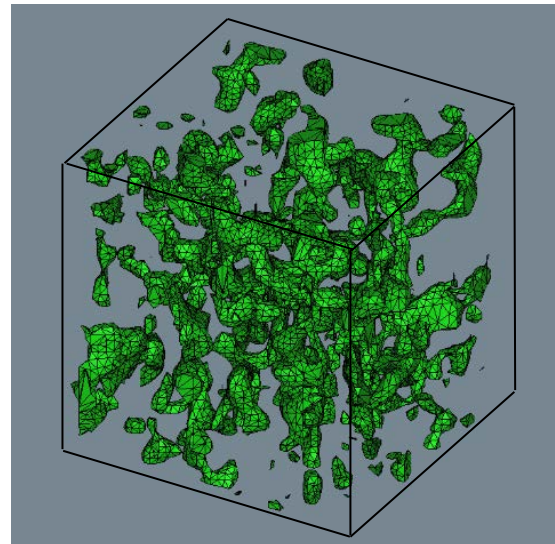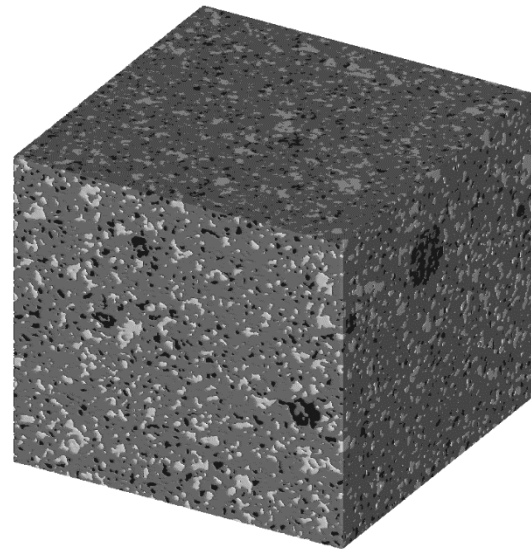

Fig. 1. (a) Reconstructed 3D microstructure (300^3 voxels) of hardened paste from X-ray CT scanned images, and (b) 3D microstructure of pore phase

The MIP technique was selected to measure smaller pore size as it can measure pore size ranging from few nanometers to 1 µm which is difficult to be measured by techniques such as BSE and micro-CT. The principle of MIP measurement is based on the assumption that the pore volume equals to the intruded volume of mercury into a porous medium. The intruded volume of mercury depends on the applied pressure. By assuming the pore geometry in cementitious material to be cylindrical, which leads to the relationship between the pore diameter d and the external applied pressure P, known as Washburn equation. The sample used for MIP was 2 ~ 3 grams taken from the bulk sample. The samples were pre-dried by heating at the temperature of 50°C prior to MIP test.

The pore size distribution was also measured by SEM with BSE for the large pore characterization. The sample size is Φ10 × 10 mm, which was cut from the bulk cylindrical specimen. The sample was first grinded and polished to obtain a flat surface prior to the BSE measurement. The images were obtained at a high vacuum with an accelerating voltage of 15 kV and the working distance of 10 ~ 15 mm. The field size was about 277 × 208 µm.

4.0   RESULTS AND DISCUSSIONS

4.1   Pore Characteristics by X-ray CT

Porosity is quantified as the fraction of void space in the volume of interest. Segmentation or image thresholding was conducted to convert the gray scale CT image to a binary image by identifying the pore space and solid matrix based on their voxel intensity values. Segmented porosity was calculated by dividing the number of pore voxels by the total number of voxels in the volume of interest.

The quantified pore size distribution from the 2D images scanned by using X-ray CT for different paste samples is shown in Fig. 2. The size of the majority of the pores ranges between 20 ~ 40 µm for pores with size greater than 3 µm which is the lower limit of the detectable pore size by the X-ray CT used in this study. The pore size of 3P samples with *w/c* ratio=0.3, including 3P-control, 3P-1d-FT, and 3P-7d-FT, is generally less than 60 µm, and the pore size is independent of the freeze-thaw cycling. Whereas, the pore size of 5P samples with *w/c* ratio=0.5 spans a wider range, particularly for sample (5P-1d-FT, 5P-7d-FT) subject to early-age freeze-thaw cycling that a large portion of the pore size is greater than 100 µm.

The quantified pore size distribution in Fig. 2 is based on the analysis of 2D images rather than the 3D image. This is because the commercial software that calculates the pore size by assuming pore shape as a sphere filling the pore space, which normally leads to an unrealistic pore size distribution compared to the real pore size distribution (Zheng *et al.* 2015).

4.2   Comparison of Pore Characteristics Measured by Different Techniques

Three techniques of MIP, BSE, and X-ray CT have been adopted in this study to characterize the pore size distribution of paste samples subject to early-age freeze-thaw cycles. The measured results are listed in Table 1 in terms of the detected pore size range

that each technique can measured and the corresponding porosity for each samples. It can be seen that BSE and X-ray CT methods can work as a complimentary method to the MIP method for measuring the pores with size greater than 1 µm, the lower limit of pore size that can be detected by BSE and X-ray CT depends on the resolution of the technique.
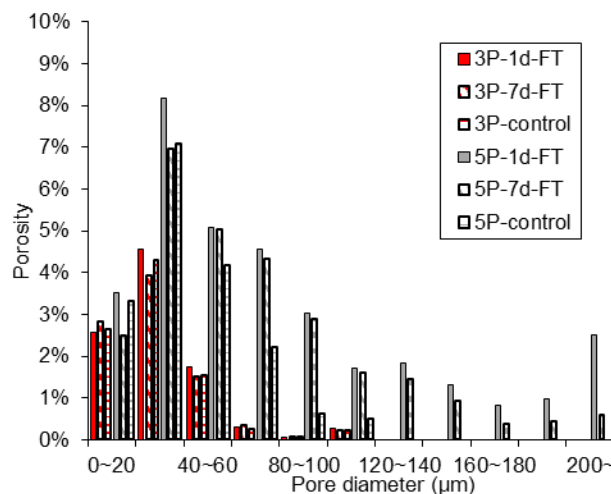

Fig. 2. Pore size distribution detected by X-ray CT for control 3P and 5P pastes and pastes subject to freeze-thaw cycling at the age of 1 and 7 days

The pore size distribution measured by the three different techniques can be plotted in one Figure across the scale of 1 nm to 100 µm as illustrated in Fig. 3. Generally, large porosity is observed for 5P sample across the pore size scales, and early-age freeze-thaw cycling causes the largest porosity. Therefore, low *w/c* ratio concrete is highly recommended to minimize the freeze-thaw damage on the porosity and the related strength and permeability issues.

It should be noted that the total porosity of sample can't be obtained by simply adding each porosity measured by using different techniques, for example, the total porosity is not equal to the summation of the porosity measured by MIP and the porosity measured by BSE or X-ray CT. This is because that MIP might overestimate the volume of the smaller pores due to the ink-bottle effect, and the image analysis based on BSE and X-ray CT might overestimate the volume of larger pores due to the limitation of resolution. The purpose of using different techniques to quantify the porosity is to compare relatively the porosity of different samples within a certain pore size range, instead of obtaining the total porosity.

Table 1. Detected pore size range and porosity by using different techniques.

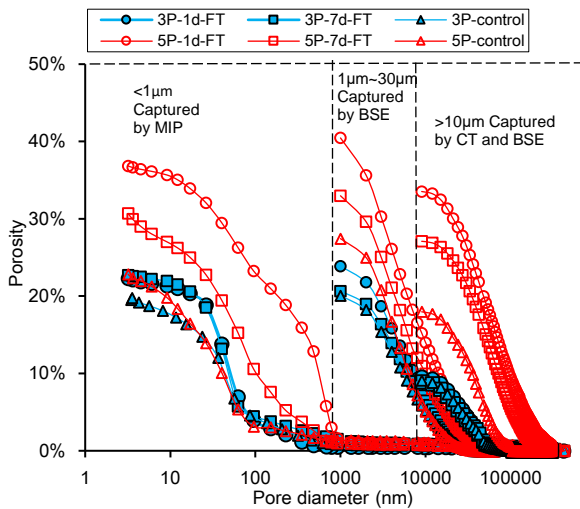| Method	Detected pore range	3P-1d-FT	3P-7d-FT	3P-control	5P-1d-FT	5P-7d-FT	5P-control
MIP	3nm~1µm	22%	24%	20%	37%	31%	23%
BSE	1µm~30µm	24%	21%	20%	41%	33%	27%
CT	10µm~	10%	9%	9%	34%	27%	18%

Fig. 3. Pore size distribution detected by MIP, BSE, and X-ray CT technique for control 3P and 5P pastes and pastes subject to freeze-thaw cycling at the age of 1 and 7 days

4.3 Computed Permeability

The calculated permeability by using Katz-Thompson relationship and Navier-Stokes method is shown in Fig. 4 for control 3P and 5P pastes and pastes subject to freeze-thaw cycling at the age of 1 and 7 days. The input pore parameters for both Katz-Thompson and Navier-Stokes methods were obtained from the X-ray CT scanned images.

It can be seen that the magnitude of the calculated permeability by Katz-Thompson relationship is about 3~4 orders of magnitude greater than that computed from Navier-Stokes method. The magnitude of calculated permeability by Katz-Thompson method is $10^{-12} \sim 10^{-10}$ m^2, while it is $10^{-16} \sim 10^{-13}$ m^2 by Navier-Stokes method. Similar trend was found by Das *et al.* (2015), they calculated the permeability of 5×10^{-14} m^2 and 5.2×10^{-16} m^2 by using Katz-Thompson and Navier-Stokes method, respectively, for the fly ash-based geopolymer with porosity of 32%.

Navier-Stokes method is more applicable to permeability prediction. First of all, the computed permeability by Navier-Stokes method is very close to the measured one and the one calculated according to other method. As measured by Nyame and Illston (1981), the permeability of paste with degree of hydration greater than 0.5 is less than 10^{-14} m^2. Garboczi and Bentz (2001) calculated the permeability based on 3D model was $10^{-15} \sim 10^{-13}$ m^2 for pastes with porosity of 20 ~ 30 %。The computed permeability ranging from $10^{-16} \sim 10^{-13}$ m^2 by using Navier-Stokes method in this study is consistent to the above values reported in the literatures, it is reasonable to conclude that Navier-Stokes method is more applicable to predict permeability of cement paste.

Moreover, the variation of the computed permeability based on Navier-Stokes method reflects the effects from the freeze-thaw cycling and the *w/c* ratio. A clear increase in permeability was observed for high *w/c* ratio paste of 5P, the increase of *w/c* ratio from 0.3 to 0.5 will increase the permeability by 2~3 orders of magnitude. The early-age freeze-thaw cycling increases the permeability by 2 orders of magnitude compared to the control sample by using Navier-Stokes method. However, the computed permeability by Katz-Thompson method does not reflect the effect from freeze-thaw cycling, and the permeability of control paste and paste subject to early-age freeze-thaw cycling is almost the same, which is not reasonable.
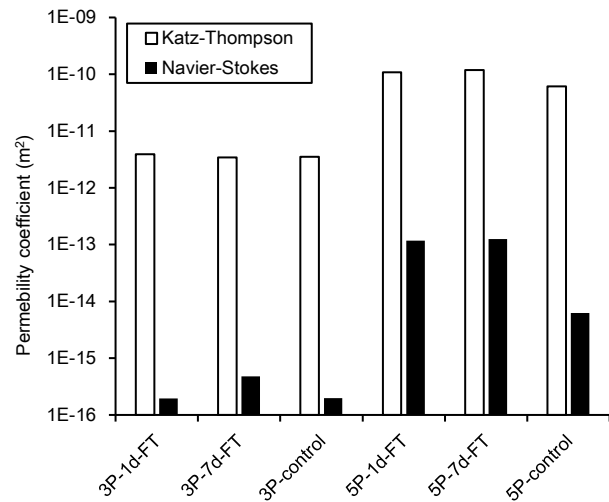

Fig. 4. Calculated permeability by Katz-Thompson and Navier-Stokes methods based on X-ray CT data for control 3P and 5P pastes and pastes subject to freeze-thaw cycling at the age of 1 and 7 days

5.0 CONCLUSIONS

The pore size distribution of paste with high *w/c* ratio of 0.5 is affected significantly by the early-age freeze-thaw cycles which causes greater porosity in all the pore size ranges. The earlier the freeze-thaw cycles, the greater the porosity in paste with high *w/c* ratio. The pore with size greater than 1 μm is significantly increased when subject to early-age freeze-thaw cycles.

Early-age freeze-thaw cycles does not affect very much the porosity of paste with low *w/c* ratio=0.3. It is recommended to use concrete with low *w/c* ratio in structures subject to severe early-age freeze-thaw cycles.

Compared to Kata-Thompson relationship, Navier-Stokes method is more applicable to predict permeability of hardened paste, as it can reflect the effects from both *w/c* ratio and the freeze-thaw cycling.

Acknowledgement

References

Bentz D P, Mizell S, Satterfield S, *et al*. 2002. The visible cement data set. Journal of Research of the National Institute of Standards and Technology, 107(2): 137.

Bentz D P, Martys N S. 2007. A stokes permeability solver for three-dimensional porous media. US Department of Commerce, Technology Administration, National Institute of Standards and Technology.

Cui L, Cahyadi J H. 2001. Permeability and pore structure of OPC paste. Cement and Concrete Research, 31(2): 277-282.

Das S, Yang P, Singh S S, *et al*. 2015. Effective properties of a fly ash geopolymer: Synergistic application of X-ray synchrotron tomography, nanoindentation, and homogenization models. Cement and Concrete Research, 78: 252-262.

Garboczi, Edward J., and Dale P. Bentz. 2001. The effect of statistical fluctuation, finite size error, and digital resolution on the phase percolation and transport properties of the NIST cement hydration model. Cement and Concrete Research, 31(10): 1501-1514.

Hu, Jing, *et al*. 2015. High-temperature failure in asphalt mixtures using micro-structural investigation and image analysis. Construction and Building Materials, 84: 136-145.

Igarashi, S., Watanabe, A., and Kawamura, M. 2005. Evaluation of capillary pore size characteristics in high-strength concrete at early ages. Cement and Concrete Research, 35: 513-519.

Katz A J, Thompson A H. 1987. Prediction of rock electrical conductivity from mercury injection measurements. Journal of Geophysical Research: Solid Earth, 92(B1): 599-607.

Nyame B K, Illston J M. 1981. Relationships between permeability and pore structure of hardened cement paste. Magazine of Concrete Research, 33(116): 139-146.

Olivier, B., Ulm, F., and Lemarchand, E., 2003. A multiscale micromechanics-hydration model for the early-age elastic properties of cement-based materials. Cement and Concrete Research, 33 (9): 1293-1309.

Promentilla M A B, Cortez S M, Papel R A D C, *et al*. 2016. Evaluation of microstructure and transport properties of deteriorated cementitious materials from their X-ray computed tomography (CT) images. Materials, 9(5): 388.

Sun X, Dai Q, Ng K. 2014. Computational investigation of pore permeability and connectivity from transmission X-ray microscope images of a cement paste specimen. Construction and Building Materials, 68: 240-251.

Zheng, H., Li, X, Liu, X. *et al*. 2015. Establishment of an immensely appraisal method for the performance test of software for material pore structure and results of preliminary practice, Chinese Journal of Stereology and Image Analysis, 20 (2): 121-127.